JSR Publications

Available Online

J. Sci. Res. **16** (2), 437-447 (2024)

JOURNAL OF SCIENTIFIC RESEARCH

www.banglajol.info/index.php/JSR

Unusual Magnetic Behaviour of Ultrafine Stable Nickel Nanoparticles

O. Mondal*

Department of Physics, M. U. C. Women's College, Burdwan, West Bengal, India

Received 6 July 2023, accepted in final revised form 27 November 2023

Abstract

Ultrafine nickel nanoparticles have been synthesized using a capping agent-assisted chemical reduction technique using two different reaction media – water and ethylene glycol. The effect of the capping agent and reaction medium concentration on the particle size and their magnetic properties have been extensively studied. The size of the nickel nanoparticles, as revealed from X-ray diffractograms and transmission electron micrographs, is less than 5 nm. The energy-dispersive X-ray spectrum confirms that the synthesized nanoparticles are pure nickel. No other element is present in the spectrum. The nanoparticles exhibit surface plasmon resonance in ultraviolet (~310 nm). The blue shift in the absorbance peak's position further confirms the particle's miniaturization. The samples should have exhibited superparamagnetic behavior because the particle size is in the nanometer range. Instead, the ferromagnetic behavior of the samples has been observed at ambient temperature, which is attributed to the formation of clusters of nanoparticles. This property makes the material applicable for data storage technology.

Keywords: Ultrafine nanoparticles; Chemical reduction technique; **f**erromagnetic.

doi: https://dx.doi.org/10.3329/jsr.v16i2.67426 J. Sci. Res. **16** (2), 437-447 (2024)

1. Introduction

Magnetic nanostructured materials have been extensively explored for scientific as well as technological interest [1,2]. Among various kinds of nanoparticles, magnetic metallic nickel is an important candidate as it exhibits interesting optical, magnetic, and catalytic properties and is suitable for different applications. Ni nanoparticles (Ni-NPs) are important for technological applications in alkaline rechargeable batteries [3], magnetic recording media [4], chemical catalysts [5,6], conducting and magnetic inks [7], ferrofluids [8], magnetic resonance imaging contrast enhancement and biomedical applications [9], antibacterial activities [10].

Various procedures for the synthesis of Ni-NPs, such as the microemulsion method [11], microwave-assisted polyol process [12,13], thermal decomposition of nickel compounds [14], chemical reduction using surfactants in both water and organic solvents [15,16] have been reported. The synthesis of Ni-NPs is relatively more complicated than that of other transition metals as they get oxidized readily. The works reported so far for

* *Corresponding author*: oindrila.rng@gmail.com

synthesizing Ni-NPs, used single or binary [17] soluble polymers as protective agents. Ni-NPs synthesized without a protective agent are also reported [15], but the same could not be an effective candidate as a ferrofluid. The works reported so far on nickel nanoparticles produced nanoparticles of size greater than 4 nm. The nickel nanoparticles synthesized by Wu et al. [11, 15] exhibited superparamagnetic behavior with coercivity of less than 10 Oe. The polymer-protected Ni-NPs [17] nanoparticles were superparamagnetic due to their small size. The saturation magnetization, remanent magnetization, and coercivity were 32 emu g^{-1}, 5.0 emu g^{-1}, and 40 Oe, respectively. For application in ferrofluids, the main challenge is to produce a stable dispersion of monodispersed anti-oxidation Ni-NPs. The smaller size of nanoparticles and narrow distribution of size favors the formation of a stable dispersion.

The main objective of the study is to synthesize nickel nanoparticles with smaller sizes and narrow size distribution in traditional fluids (water, ethylene glycol) using a chemical reduction technique. Though the process is very well-known, by introducing cationic surfactant cetyltrimethylammonium bromide (CTAB) and varying its concentration in solution, we are successful in producing narrow-dispersed Ni-NPs with the size of the order of single domain. This method can be an efficient way of synthesizing ferrofluids in one step. The synthesized nanoparticles exhibit interesting and unusual magnetic properties due to the clustering of individual Ni-NPs. The magnetic properties of samples synthesized in different reaction media (water and ethylene glycol) and with different CTAB concentrations are compared.

2. Experimental Details

2.1. *Materials*

The precursors nickel chloride ($NiCl_2.6H_2O$), hydrazine hydrate ($N_2H_4.H_2O$), ammonia solution (NH_4OH), sodium borohydride ($NaBH_4$), ethylene glycol (EG) and cationic surfactant CTAB [$(C_{16}H_{33})N(CH_3)_3Br$] were procured from Merck (Germany). All the reagents were of analytical grade and used without further purification.

2.2. *Methods*

The Ni-NPs were synthesized using the chemical reduction method [18]. The precursor nickel chloride (0.05M) was added to water containing 10 mM CTAB. The pH of the solution was maintained at around 10 using an ammonia solution. After the addition of the reducing agent hydrazine hydrate to the nickel salt solution, it was stirred continuously and heated at 333 K. As the reduction was incomplete, a small amount of sodium borohydride (0.01 g) was added. The solution turned black, indicating the completion of the reduction process. The solution was then cooled to room temperature to collect the particles by centrifugation. The particles, dried in a vacuum, were used for further characterization. The solution of nickel chloride in EG with different CTAB concentrations (5 and 10 mM) was also taken to study the effect of the reaction media and

CTAB concentration. The samples are designated as SW, SEG5, and SEG10 for samples synthesized in water and EG with CTAB concentrations of 5 mM and 10 mM, respectively.

2.3. *Characterization*

Detailed structural and morphological characterization of the dried samples have been performed using the X-ray diffraction (XRD) technique and transmission electron microscope (TEM). We have used Bruker D8 X-Ray diffractometer, equipped with 0.1542 nm CuKα radiation, to obtain the XRD pattern. The morphology of the samples was investigated using TEM (JEOL Model JEM 2010) operated at an accelerating voltage of 200 kV and equipped with a detector for energy-dispersive X-ray (EDX) analysis. Cary 5000 UV-Vis-NIR spectrophotometer, manufactured by Agilent Technologies, has been used for the optical characterization of the samples. The samples' Curie temperatures (TC) were obtained from a thermal magnetic analysis (TMA) curve measured using TA Instruments SDT Q600. Magnetic measurements were carried out using the MPMS superconducting quantum interference device (SQUID) magnetometer (supplied by Quantum Design, USA) over the 2–300 K temperature range.

3. Results and Discussion

3.1. *Crystal structure study*

Fig. 1 shows the X-ray diffractograms of the synthesized samples SW, SEG5, and SEG10. The peaks are well assigned to the cubic phase of nickel [JCPDS card no-04-0850]. The absence of any extra peak proves the purity of the samples. Also, it is noticeable that the XRD pattern of SEG5 and SEG10 shows peak broadening compared to SW. This confirms the formation of smaller crystallites in EG media. As calculated using the Debye Scherer formula, the crystallite sizes are 9.73, 6.02, and 5.75 nm for SW, SEG5, and SEG10, respectively.

The software Material Analysis Using Diffraction (MAUD) was used for Rietveld's refinement of the XRD data of the three samples [19]. As obtained from the refinement, the samples' lattice parameters are 3.5292, 3.5280, and 3.5239 Å (lattice constant of bulk Ni~ 3.523 Å). The crystallite sizes extracted from Rietveld analysis are 9.59, 6.74, and 4.54 nm for SW, SEG5, and SEG10 respectively. From XRD analysis, it is very clear that EG medium is effective for the production of particles with smaller sizes. The crystallite size in EG medium is smaller compared to that of aqueous medium because of the reducing property of glycol. Moreover, EG also inhibits the growth of nanoparticles in a similar fashion as a capping agent does. It was also observed that the crystallite size was smaller with a CTAB concentration of 10 mM. Increasing the concentration of the capping agent accelerates the production of smaller particles.

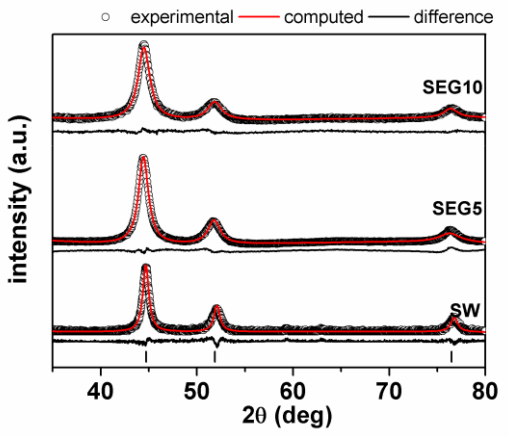

Fig. 1. XRD pattern of Ni-NPs synthesized under different conditions along with Rietveld fit.

3.2. *Morphological study*

The typical micrograph of the sample SEG10 is presented in Fig. 2 (a). The sample consists of ultrafine Ni-NPs of narrow size distribution. The particle size distribution of sample SEG10 and log-normal fit are presented in Fig. 2(b). The average particle size obtained from log-normal fit is 2.5 nm with a standard deviation of 1.03 nm.

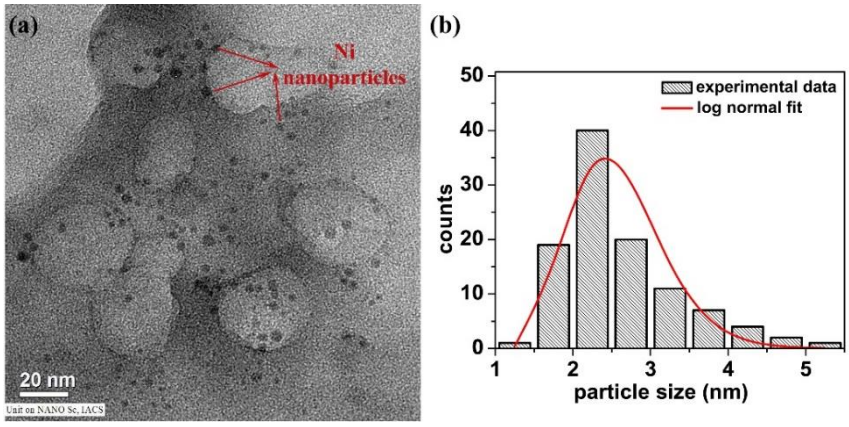

Fig. 2. (a) TEM images of the sample SEG10. (b) Particle size distribution of the sample with log-normal fit.

Fig. 3 (a) presents the micrograph of the sample SW. It clearly shows that the sample is in the form of clusters comprising smaller particles. The average size of the clusters is ~30 nm. The TEM image confirms that the appropriate parameters to synthesize monodispersed Ni-NPs are EG solvents with 10 mM CTAB at 333 K. The selected area diffraction (SAED) is presented in Fig. 3 (b), proving the sample's polycrystallinity. The d

value calculated from the rings of the SAED pattern matches with the interplanar spacings of Ni.

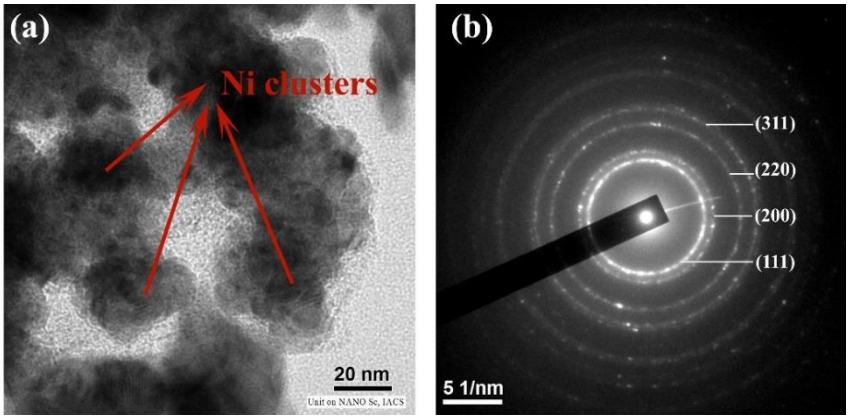

Fig. 3 (a) TEM image, (b) SAED pattern of sample SW.

The EDX spectrum of sample SW is presented in Fig. 4 to visualize the elemental composition. It confirms that the synthesized particles comprise pure nickel. The elements C and Cu arise from the carbon-coated copper grid on which the sample for TEM was cast.

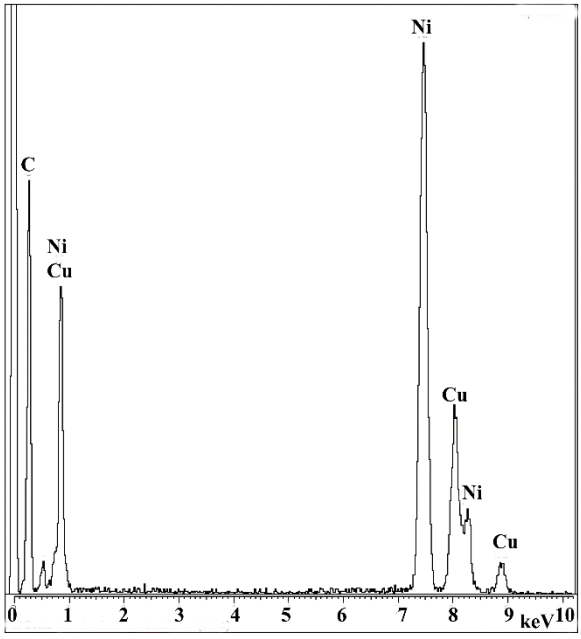

Fig. 4. EDX spectrum of sample SW.

3.3. *UV-visible absorbance spectroscopy*

When visible electromagnetic radiation is incident on metal nanoparticles, there is a resonant oscillation of conduction electrons at the surface. This phenomenon is called the surface plasmon resonance (SPR). The peak in the optical absorbance spectrum of metal nanoparticles corresponds to absorbance due to SPR. The optical absorbance spectrum of the sample SEG10 is presented in Fig. 5.

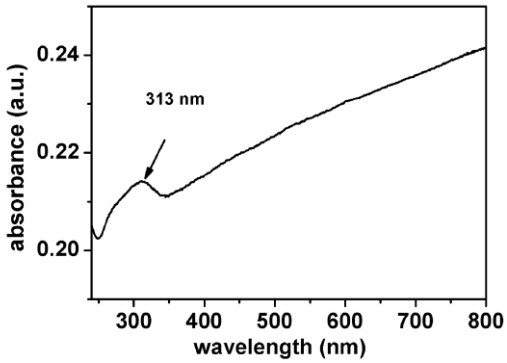

Fig. 5. Optical absorbance spectrum of SEG10 dispersed in ethanol.

The absorption spectrum peaked at 313 nm, corresponding to the SPR of Ni NPs [20]. The spectrum shows a shift in the position of the absorbance peak towards the lower wavelength region, as compared to the reported value. The shift is attributed to the quantum confinement effect, which confirms nanosized particles' presence. We attempted to estimate the average particle size from absorbance data using the Mie scattering formula,

$$r_{metal} = \frac{v_F}{2\pi c\left(\frac{\Delta\lambda}{{\lambda_p}^2}\right)} \quad (1)$$

where, V_F is taken equal to 2.33×10^6 m $s^{-1,}$ which is the value of Fermi velocity of Ni NPs at room temperature, c is the velocity of light in vacuum, λ_p is the wavelength at which SPR occurs, and $\Delta\lambda$ is the value of full width at half maximum of the absorbance peak. The average radius of Ni-NPs is calculated using the equation. (1) is 1.51 nm, which is in good agreement with the particle size obtained from TEM and Rietveld analysis.

3.4. *Thermal study*

The magnetic Curie temperature (T_C) of samples can be measured from a Thermal Magnetization Analyzer (TMA). In TMA, the thermogravimetric curve of the sample under investigation is measured in an inhomogeneous magnetic field, generally from a permanent magnet, placed on the top of the furnace directly over the test specimen. The TMA curve of the sample SEG10 measured in the inert atmosphere of nitrogen is

presented in Fig. 6. The major weight loss in the TG curve that starts around 520 K corresponds to the decomposition of the CTAB layer on the nanoparticles. The temperature at which an increase in weight occurs corresponds to the transition temperature from the ferromagnetic to paramagnetic phase (T_C). The T_C for the corresponding sample is 613 K (T_C of bulk Ni~ 631 K). Compared to the bulk, the decreased value of TC is attributed to the smaller size of synthesized Ni-NPs. The fact that the increase in weight can be due to oxide phase formation is discarded, as the experiment was conducted in an inert nitrogen atmosphere. The TMA curve proves the ferromagnetic nature of the sample at room temperature.

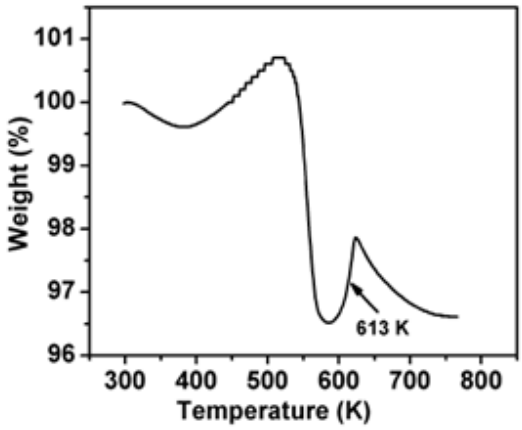

Fig. 6. TMA curve of the SEG10 in N_2 atmosphere.

3.5. *Magnetic study*

Fig. 7 depicts the variation of magnetization with temperature under field-cooled (FC) and zero-field-cooled (ZFC) conditions at 50 Oe. The FC-ZFC curves of all the samples showed bifurcation up to room temperature and a weak hump in the low-temperature region (6-18 K). The position of the hump in SW, SEG5, and SEG10 are 11.6, 18.2, and 6.8 K. The FC magnetization curve remains almost independent throughout the temperature range.

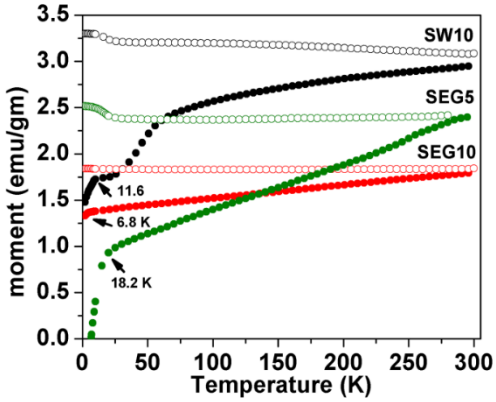

Fig. 7. Plot of magnetization with temperature under ZFC- FC condition of the synthesized samples.

The plot of magnetization (M) with the applied magnetic field (H) for the sample SEG10 at different temperatures is presented in Fig. 8. The sample showed ferromagnetic behavior in the whole temperature range (2-300 K), which is quite unusual for these ultrafine Ni-NPs. The inset presents the magnified view of low-field data to show the coercivity of the sample at different temperatures. For bulk Ni, the saturation magnetization, remanent magnetization, and coercivity values at 300 K are about 55 emu/g, 2.7 emu/g, and 100 Oe, respectively [21]. In our sample, the corresponding values are 38.6 emu/g, 11.96 emu/g, and 140.6 Oe at 300 K. The reason behind the 30% decrease in the value of M_S is the nano dimension of the sample. In our case, as CTAB is used as a protective agent, the interaction of surface atoms with CTAB is another reason behind the decrease of M_S. Generally, the coercivity reduces to zero (superparamagnetism) in the nano regime, but we observe an increased value of H_C (compared to bulk) in our sample. The reason behind such a peculiar observation is yet to be understood. The increased value of coercivity makes it technologically applicable for data storage.

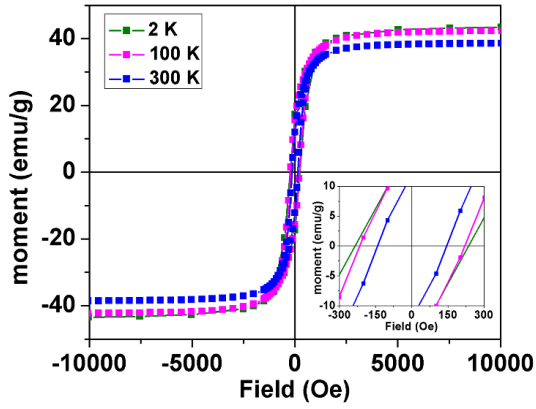

Fig. 8. Hysteresis loops of sample SEG10.

The variation of the coercivity (H_C) and saturation magnetization (M_S) of the sample SEG10 with temperature (T) is presented in Fig. 9. The equation $25KT_B = K_{eff}V$ is used for calculation of Blocking temperature (T_B), where K is Boltzmann's constant, V is the volume of the nanoparticle, K_{eff} is anisotropy constant assumed to be 15.6×10^5 erg cm^{-3} for particles with size 3.7 nm [22]. Using the above information, the blocking temperature for the sample SEG10 is calculated to be 6.5 K which is almost equal to the position of the hump in the ZFC curve for the sample (6.8 K). Accordingly, the hump in the ZFC curve can be considered as the signature of blocking.

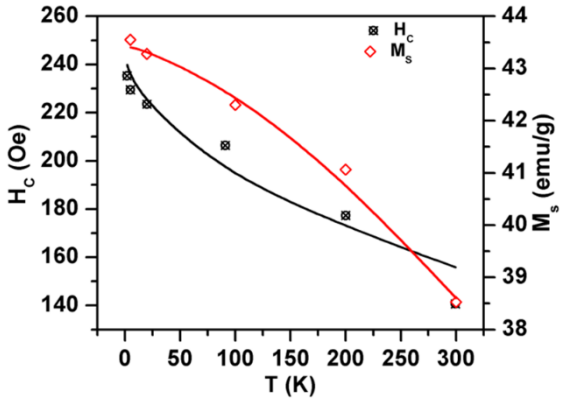

Fig. 9. Variation of H_C and M_S with temperature T (black and red lines are drawn to guide the eye).

Ferromagnetic metals show superparamagnetism (SPM) when their domain size goes down to the nanometer range. Depending upon the size, the blocking temperature varies and generally appears at low temperatures. In contrast, ultrafine Ni-NPs demonstrate ferromagnetic behavior with definite coercivity even at ambient temperature. Though a signature of blocking is reflected in the ZFC curve, the value of blocking temperature matches the theoretically estimated value. The interaction of surface atoms with the surfactant may play an important role. However, we strongly believe that clusters of ultrafine Ni-NPs (quite big in size), which is clear from the TEM study, are responsible for the observed ferromagnetism at ambient temperature. It is established that blocking temperature increases with particle size and could be above room temperature for bigger size. The bigger size clusters are responsible for ferromagnetic behavior at room temperature. Though very rare, the appearance of ferromagnetism at ambient temperature for such smaller particle size has been reported for cobalt-graphene nanocomposite [23]. They attributed this to cobalt nanoparticles' strong dipolar magnetic interaction separated by a graphene layer.

4. Conclusion

In summary, narrow-dispersed ultrafine nickel nanoparticles with an average size of 2.5 nm have been synthesized by hydrazine hydrate-sodium borohydride reduction. The

particle size can be controlled by modulating the solvent and surfactant concentration. The blue shift in the position of the absorbance peak due to SPR is attributed to the nano dimension of the nanoparticles. In contrast, the synthesized Ni-NPs show ferromagnetic behavior even up to ambient temperature, which is quite unusual. The presence of room-temperature ferromagnetic behavior in single-domain particles makes the material an effective candidate for data storage. As the synthesized nickel nanoparticles have both properties, they will find applications in data storage.

Acknowledgments

The author thanks M. Pal, CSIR-Central Glass and Ceramic Research Institute, Kolkata, for his constant support, guidance, and fruitful discussions related to the present work. The author thanks the unit on Nanoscience, Indian Association for the Cultivation of Science, Jadavpur, for providing the experimental facilities required to carry out the work.

References

1. S. Negi, A. Sharma, and P. Sharma, J. Sci. Res. **12**, 555 (2020). https://doi.org/10.3329/jsr.v12i4.46052
2. A. Farzin, S. A. Etesami, J. Quint, A. Memic, and A. Tamayol, Adv. Healthc. Mater. **9**, ID 1901058 (2020). https://doi.org/10.1002/adhm.201901058
3. H. Wang, Y. Liang, M. Gong, Y. Li, W. Chang, et al., Nat. Commun. **3**, 917 (2012). https://doi.org/10.1038/ncomms1921
4. S. Edel'man, D. A. Petrov, R. D. Ivantsov, S. M. Zharkov, R. I. Khaibullin, et al., J. Expt. Theoret. Phys. **113**, 1040 (2011). https://doi.org/10.1134/S1063776111160035
5. Q. Cheng, C. Wu, J. Chen, Y. Zhou, and K. Wu, J. Phys. Chem. C **115**, 22845 (2011). https://doi.org/10.1021/jp207442u
6. L. –R. Zhang, J. Zhao, M. Li, H. –T. Ni, J. –L. Zhang, et al., New J. Chem. **36**, 1108 (2012). https://doi.org/10.1039/c2nj20690k
7. W. J. Tseng and C-N Chen. J. Mater. Sci. **41**, 1213 (2006). https://doi.org/10.1007/s10853-005-3659-z
8. A. P. R. Mary, C. S. S. Sandeep, T. N. Narayanan, R. Philip, P. Moloney, et al., Nanotechnology **22**, ID 375702 (2011). https://doi.org/10.1088/0957-4484/22/37/375702
9. D. Guo, C. Wu, J. Li, A. Guo, Q. Li, et al., Nanoscale Res. Lett. **4**, 1395 (2009). https://doi.org/10.1007/s11671-009-9411-x
10. M. R. Ahghari, V. Soltaninejad, and A. Maleki, Sci. Rep. **10**, 12627 (2020). https://doi.org/10.1038/s41598-020-69679-4
11. D. –H. Chen and S. –H. Wu, Chem. Mater. **12**, 1354 (2000). https://doi.org/10.1021/cm991167y
12. D. Li and S. Komarneni, J. Am. Ceram. Soc. **89**, 1510 (2006). https://doi.org/10.1111/j.1551-2916.2006.00925.x
13. R. Eluri and B. Paul, Mater. Lett. **76**, 36 (2012). https://doi.org/10.1016/j.matlet.2012.02.049
14. Y. Chen, D. –L. Peng, D. Lin, and X. Luo, Nanotechnol. **18**, ID 505703 (2007). https://doi.org/10.1088/0957-4484/18/50/505703
15. S. –H. Wu and D. –H. Chen, J. Colloid Interface Sci. **259**, 282 (2003). https://doi.org/10.1016/S0021-9797(02)00135-2
16. G. Cardenas and J. Acuna, Colloid Polym. Sci. **279**, 442 (2001). https://doi.org/10.1007/s003960000440

17. D. –H. Chen and C. –H. Hsieh, J. Mater. Chem. **12**, 2412 (2002). https://doi.org/10.1039/b200603k
18. O. Mondal, A. Datta, D. Chakravorty, and M. Pal, MRS Commun. **3**, 91 (2013). https://doi.org/10.1557/mrc.2013.13
19. L. Lutterotti, MAUD, version 2.07, (2008).
20. J. Zhang and C. Q. Lan, Mater. Lett. **62**, 1521 (2008). https://doi.org/10.1016/j.matlet.2007.09.038
21. J. H. Hwang, V. P. Dravid, M. H. Teng, J. J. Host, B. R. Elliott, et al., J. Mater. Res. **12**, 1076 (1997). https://doi.org/10.1557/JMR.1997.0150
22. Y. Hou and S. Gao, J. Mater. Chem. **13**, 1510 (2003). https://doi.org/10.1039/b303226d
23. Z. Ji, X. Shen, Y. Song, and G. Zhu, Mater. Sci. Eng. B **176**, 711 (2011). https://doi.org/10.1016/j.mseb.2011.02.026